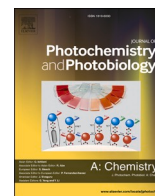




Contents lists available at ScienceDirect

Journal of Photochemistry & Photobiology, A: Chemistry

journal homepage: www.elsevier.com/locate/jphotochem

Synthesis of new Zn (II) complexes for photo decomposition of organic dye pollutants, industrial wastewater and photo-oxidation of methyl arenes under visible-light

Jakeer Ahemed^a, Jakeer Pasha^a, Venkateshwar Rao D^a, Ranjith Kore^a, Ramesh Gade^a, Yadagiri Bhongiri^{a,*}, Prabhakar Chetti^b, Someshwar Pola^{a,*}

^a Department of Chemistry, Osmania University, University College of Science, Hyderabad, Telangana, India

^b Department of Chemistry, National Institute of Technology, Kurukshetra, Haryana, India

ARTICLE INFO

Keywords:

Photocatalysis
Zn(II) complexes
Organic pollutants
Photo-fragmentation
Food industrial wastewater
Photooxidation

ABSTRACT

Synthesis of new Schiff's base Zn-complexes for photo-oxidation of methyl arenes and xylenes are reported under visible light irradiation conditions. All the synthesized new ligands and Zn-complexes are thoroughly characterized with various spectral analyses and confirmed as 1:1 ratio of Zn and ligand with distorted octahedral structure. The bandgap energies of the ligands are higher than its Zn-complexes. These synthesized new Zn(II) complexes are used for the photo-fragmentation of organic dye pollutants, photodegradation of food industrial wastewater and oxidation of methyl arenes which are converted into its respective aldehydes with moderate yields under visible light irradiation. The photooxidation reaction dependency on the intensity of the visible light was also studied. With the increase in the dosage of photocatalyst, the methyl groups are oxidized to get aldehydes and mono acid products, which are also identified from LC-MS data. Finally, [Zn(PPMHT)Cl] is with better efficiency than [Zn(PTHMT)Cl] and [Zn(MIMHPT)Cl] for oxidation of methyl arenes is reported under visible-light-driven conditions.

1. Introduction

The Schiff's base metal complexes are used in wide range of applications, which includes photocatalysis [1–3], biomedical [4], and material science [5]. In the Schiff's base, imine bond play a vital role in the formation of the metal complexes with a variety and various donor atoms. The ligands containing amide and imine functional groups are very significant in the formation of broad range of metal complexes for various applications [6,7]. Some of the Schiff's base complexes of Ti (IV), Ni (II), Cu (II) and Zn (II) are known for photodegradation of dyes like methylene blue (MB) under visible-light-driven conditions [8–11].

The waste water obtained from various industries such as textiles and pharmaceuticals, is a major challenging task for the storage, purification and reusable system. The dyes contaminated with the water is directly effects both aquatic and soil environments. For the purification of waste water, different methods are developed in the presence of UV light irradiation techniques [12]. Mono and bimetallic complexes [13], binary and ternary metal oxides [14,15] are known for the degradation of dyes under UV or visible light irradiation. However, the activity of metal

organic frameworks depends on the surface area, bandgap energy, purity, thermal and photostability properties [16]. In the case of Schiff's base metal complexes with simple ligands coordinated with variable metal ions are known for the reduction in the bandgap energy as compared with other ligands and pure metal oxides [16]. Due to reduction in its bandgap, Schiff's base complexes are useful in the photodegradation of simple methylene blue dye under visible-light conditions [17]. However, these metal complexes were not used for the degradation of methyl orange (MO) and methyl violet (MV). Therefore, we designed and synthesized new Schiff's base Zn (II) metal complexes for the photo-fragmentation of both anionic and cationic dyes such as MO [18] and MV [19] respectively. Moreover, based on outcomes obtained from photo decomposition of organic dye pollutants (ODPs) and food industrial wastewater (FIWW), it is also reported the photooxidation of methyl arenes [20].

2. Experimental section

All the reagents such as ZnCl₂·2H₂O, 2-bromo-1-phenylethanone,

* Corresponding authors.

E-mail address: somesh.pola@gmail.com (S. Pola).

<https://doi.org/10.1016/j.jphotochem.2021.113455>

Received 28 May 2021; Received in revised form 29 June 2021; Accepted 15 July 2021

Available online 21 July 2021

1010-6030/© 2021 Elsevier B.V. All rights reserved.

hydrazinecarbothioamide, methyl arenes, 2-hydroxybenzaldehyde and solvents were acquired from Sigma-Aldrich and used without further purification.

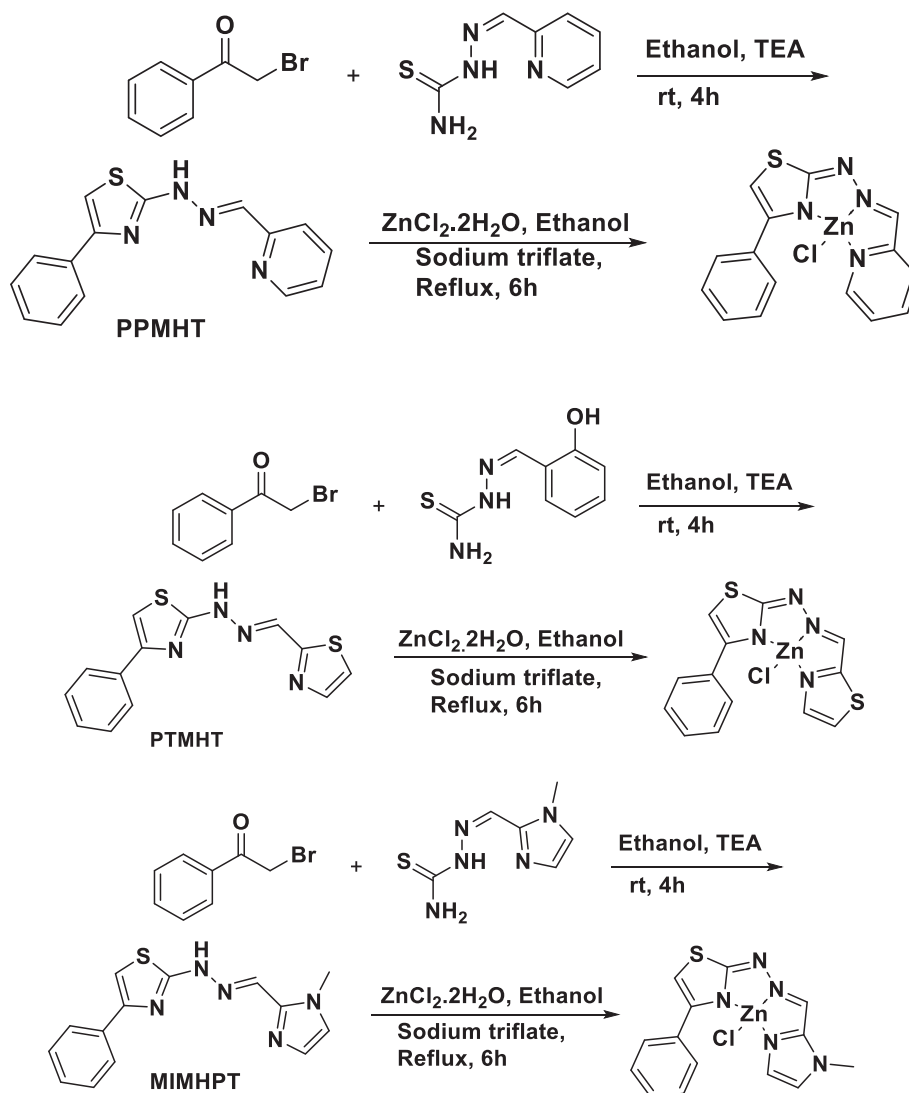
2.1. Preparation of ligands and Zn (II) complexes

Ligands are synthesized by using known methods [21] and preparation of Zn (II) complexes with these synthesized ligands are described in in [supplementary information](#). The synthesis of reported ligands and Zn (II) complex structures are shown in [Scheme 1](#).

2.2. Characterization techniques for analysis of Zn (II) complexes

The Bruker UltrafleXtrema MALDI-TOF/TOF Mass Spectrometer is used for the estimation of molecular mass of Zn(II) complexes. Thermograms of all the samples were obtained using Shimadzu differential thermal analyzer (DTG-60H) with a heating rate of $10\text{ }^{\circ}\text{C min}^{-1}$ with Temperature Program range from $50\text{ }^{\circ}\text{C}$ to $1000\text{ }^{\circ}\text{C}$ at Nitrogen atmosphere with a purge rate of 20 mL/minute . The room temperature powder X-ray diffractograms of ZnO residue were recorded using Rigaku powder X-ray diffractometer (Cu $K\alpha$, $\lambda = 1.5406\text{ \AA}$) in the 2θ range $10 - 80^{\circ}$ for established the ZnO phase with reported JCPDF data. FT-IR spectra were recorded using Shimadzu spectrometer in the form of

KBr pellets with 4 cm^{-1} resolution. ^1H NMR spectra recorded on a Bruker AV400 MHz Spectrometer with chemical shifts referenced using the ^1H resonance of residual d_6 -DMSO. Melting points verified on a Cintex apparatus. Brunauer-Emmett-Teller (BET) surface areas were determined by nitrogen adsorption-desorption isotherm measurements at 77 K on a Quantachromeautosorb automated gas sorption system. The electronic spectra were obtained in chloroform solutions on a JASCO V-650 UV-Visible spectrophotometer. The surface morphology and cross-section images of the devices were taken by field-emission scanning electron microscopy (FE-SEM, ULTRA PLUS, a member of Carl Zeiss). The photoluminescence (PL) spectra of the catalysts were recorded on a HORIBA Scientific Fluorescence Spectrophotometer, and the samples were excited at their respective excitation with slit width 2 nm . Cyclic voltammetry tests were performed on a PC-controlled CHI 620C electrochemical analyzer in a $\text{CH}_3\text{CN}/\text{C}_2\text{H}_4\text{Cl}_2$ solvent at a scan rate of 100 mVs^{-1} using NBu_4PF_6 (0.1 M) as the supportive electrolyte. The standard calomel electrode (SCE), glassy carbon, and platinum wire were used as a reference, working, and counter electrodes, respectively. All the photo-fragmentation reactions were conducted through a multi-tube photo-reactor system with tungsten visible light, Lelesil Innovative Systems, India.



Scheme 1. Synthesis of new ligands and Zn (II) complexes.

2.3. Photo-fragmentation of various organic dye pollutants (ODPs)

The catalyst (new Zn (II) complexes) (50 mg) was placed in an aqueous solution of ODP (10^{-4} M, 50 mL) in an 80 mL cylindrical quartz glass reactor. The photo-fragmentation of ODP was studied under visible light (300 Watts Tungsten lamp with photon flux of 6.42×10^8 Einstein/s) for 180 min. Before irradiation and sampling, adsorption-desorption pre-equilibrium of the dye was accomplished in the dark for a period of 60 min. Samples were collected at every 30 min interval and the suspended catalyst particles were separated through a Millipore filter and then estimated by UV-Vis spectrophotometer at respective λ_{max} .

2.4. Photo decomposition of food industrial wastewater (FIWW)

The Zn (II) complex (photocatalyst) (100 mg) was distributed in 500 mL of FIWW in a 1000 mL cylindrical quartz glass photoreactor. The photo decomposition of FIWW was supported out under visible light (300 Watts Tungsten lamp with photon flux of 6.42×10^8 Einstein/s) for 180 min. The FIWW solution kept dark under 60 min. for achieving of adsorption-desorption equilibrium. After removal of the photocatalyst particles through a Millipore Membrane filter (0.24 μm pore size), every 30 min. of time interval, collected the sample and characterized through UV-vis and LC-MS spectra.

2.5. Photo-oxidation of methyl arenes

25 mg of photo-catalyst was placed in 10 mmol of methyl arene in a 10 mL cylindrical quartz glass reactor. Then 25 mg of superoxide or hydroxyl radical scavengers (benzoquinone (BQ) / t-butyl alcohol (TB)) was added [22]. The photo-oxidation experiments were carried out under visible light (300 Watts Tungsten lamp) for 8 h [13]. The reaction mixture was monitored with TLC. After completion of reaction, the photo-catalyst was filtered and washed with distilled water and extracted by using ethyl acetate. The crude products were purified by simple filter column to yield pure aldehydes (Scheme 2) with 70 to 85% yields.

3. Results and discussion

The physicochemical and analytical data of all the metal (II) complexes with new ligands PPMHT, PTMHT and MIMHPT are given in Table 1. The experimental results of elements C, H, N and metal are in good agreement with the values calculated for the formulae [Zn (PPMHT)(Cl)], [Zn(PTMHT)Cl] and [Zn(MIMHPT)Cl]. The mass spectra of both the ligands and Zn (II) complexes (Figs. S1-S6) were confirmed by using maldi (TOF) technique and the high mass peak was assigned as $[\text{ZnL}(\text{Cl})]^+$ (L = PPMHT, PTMHT and MIMHPT). The molar conductance values of all the complexes were specific in N, N-dimethylformamide at 10^{-3} M concentration and the results are presented in Table 1. The molar conductance values between 10.99, 11.43 and 12.36 $\text{O}^{-1}\text{cm}^2\text{mol}^{-1}$ indicative of that all the complexes were non-electrolytes [23]. The conductance values are unaffected even after 48 h, confirmed that, there is no perceptible ionization and strong interactions between the metal ion, PPMHT or PTMHT or MIMHPT ligand and the chloride ions. Therefore, the mass spectral data, analytical data and molar conductance confirms the formulae of the complexes as [Zn(PPMHT)Cl], [Zn(PTMHT)Cl] and [Zn(MIMHPT)Cl] [22].

The thermal decomposition and stabilities of all the Zn-complexes



Scheme 2. Photooxidation of methyl arenes in the presence of Zn (II) complexes under visible light irradiation.

were studied to find out their relative thermal stability and decomposition characteristics [24]. The TGA data of all the complexes were achieved under N_2 atmosphere between 50 and 1000 $^\circ\text{C}$ at a heating rate of $10^\circ\text{C min}^{-1}$ and shown in the Fig. 1. The thermograms of all three Zn-complexes exhibit decomposition in a single stage due to coordinated ligand part and chloride ions. In the decomposition stage, ligand part was lost in the temperature range of 350–550 $^\circ\text{C}$. After decomposition, the residue left in the crucible is confirmed as nano particle of ZnO [25]. The obtained residue of ZnO powder was tested with the Powder X-ray diffraction (P-XRD) and shown in Fig. S7. The P-XRD peaks are matched with JCPDS data (Card No: 36–1415) [26].

The bonding mode of the ligand was elucidated by comparing the IR spectra of ligands PPMHT or PTMHT or MIMHPT and its Zn (II) complexes, shown in Fig. S8. For the ligands, narrow strong bands appeared in the IR spectra at 2862 – 2968 cm^{-1} , and is assigned as symmetric and asymmetric $\nu(\text{C}-\text{H})$ stretching modes of the alkyl group. The strong band observed at 1682 cm^{-1} in the spectrum of PPMHT are attributed to the stretching vibration of the imine nitrogen ($\text{Ar}-\text{N}=\text{C}-$) [29]. The band due to the imine nitrogen also shifted to lower in the frequencies (1632–1626 cm^{-1}) in all the complexes indicating its coordination with imine nitrogen. Similarly, coordinated water peaks were identified and also imine peaks were moved to lower frequencies in Zn (II) complexes of PTMHT and MIMHPT ligands. The two new vibronic modes in the far-IR spectra of complexes, one around 434 cm^{-1} and the other around 312 cm^{-1} are also observed and are due to $\nu(\text{Zn}-\text{N})$ and $\nu(\text{Zn}-\text{Cl})$ [22,27] respectively. These vibrational modes in the infrared spectra of complexes indicating that the Zn (II) ion is coordinated to the PPMHT/PTMHT/MIMHPT ligands through aromatic ring nitrogen, imine nitrogen atoms and one hydroxyl group. The IR spectral absorptions of Zn (II) complexes are shown in Fig. S8. Therefore, the complexation of Zn^{2+} ion with ligand PPMHT or PTMHT or MIMHPT through the nitrogen of thiazole via tautomerism, heterocyclic ring and imine along with one chloride ion directly bonded to Zn^{2+} ion. Which is supported by low conductance value of the complexes, which reveal that the anion chloride is coordinated with the metal ion.

The ^1H NMR spectra of diamagnetic Zn-complexes were recorded in d_6 -DMSO at room temperature. The resonance signals (δ ppm) of different types of protons in the Zn (II) complexes and representative spectra are shown in Figs. S9 to S14. The azomethine proton resonance signal observed at 8.72 ppm in the spectrum of ligand PPMHT and it is shifted to down field side by 0.15–0.20 ppm in its Zn(II) complex, which indicates that the nitrogen atoms are coordinated to Zn(II) metal ion [22]. Similarly, ^1H NMR spectra of other two Zn (II) complexes with respective ligand clearly shifted the peaks which indicated that Zn (II) ions were strongly complexed with ligand and highly stable. Based on above analysis the tentative structures of the Zn (II) complexes are shown in Fig. S15.

The solution phase UV-vis spectra of ligands and Zn (II) complexes are shown in Fig. 2a and b. In Zn (II) complexes all the absorption bands shifted to higher wavelength side as compared to ligands (PPMHT, PTMHT and MIMHPT), given in Table 2. In the reported complexes, the heteroatoms have the additional non-bonding electrons, which assists more active delocalized electrons in heterocyclic systems of the thiazole derivatives and hence the λ_{max} values of thiazole-based Zn (II) complexes are moved to a higher wavelength region than ligands. Therefore, bandgap energy is decreased due to intramolecular metal-ligand charge transfer within entire complex [28]. The bandgap energy values are also presented in the Table 2.

Solid state UV-vis-DRS spectra of ligands and complexes were examined and given in Table 2 and shown in Fig. 2c and d. The absorption bands are shifted towards higher wavelength region by 50 to 70 nm, due to strong overlapping of orbitals in solid phase than solution phase.

The HOMO-LUMO gap energies of ligands and complexes in solution (DMF) and solid phases were almost equal which indicated the metal-ligands charge transfer (MLCT) was same.

Table 1
Elemental, mass spectral and molar conductivity information of ligands and complexes.

Compound	% Yield	^a M.P/D.P. (°C)	%C (calcd)	%H (calcd)	%Cl (calcd)	%N (calcd)	%S (calcd)	%Zn (calcd)	Λ_m ohm ⁻¹ mol ⁻¹ cm ² (DMF)
PPMHTC ₁₅ H ₁₂ N ₄ S	65	178	64.23 (64.26)	4.28 (4.31)	—	19.93 (19.99)	11.41 (11.44)	—	—
PTMHTC ₁₃ H ₁₀ N ₄ S ₂	72	144	54.48 (54.52)	3.49 (3.52)	—	19.51 (19.56)	22.34 (22.39)	—	—
MIMHPTC ₁₄ H ₁₃ N ₅ S	59	159	59.29 (59.34)	4.58 (4.62)	—	24.68 (24.72)	11.28 (11.31)	—	—
[Zn(PPMHT)Cl] C ₁₅ H ₁₁ ClN ₄ SZn	71	254	47.35 (47.39)	2.89 (2.92)	9.27(9.32)	14.69 (14.74)	8.39(8.43)	17.16 (17.20)	10.99
[Zn(PTMHT)Cl] C ₁₃ H ₉ ClN ₄ S ₂ Zn	58	306	40.39 (40.43)	2.32 (2.35)	9.14(9.18)	14.47 (14.51)	16.56 (16.60)	16.87 (16.93)	11.43
[Zn(MIMHPT)Cl] C ₁₄ H ₁₂ ClN ₅ SZn	52	306	43.86 (43.88)	3.13 (3.16)	9.23(9.25)	18.24 (18.28)	8.34(8.37)	17.02 (17.06)	12.36

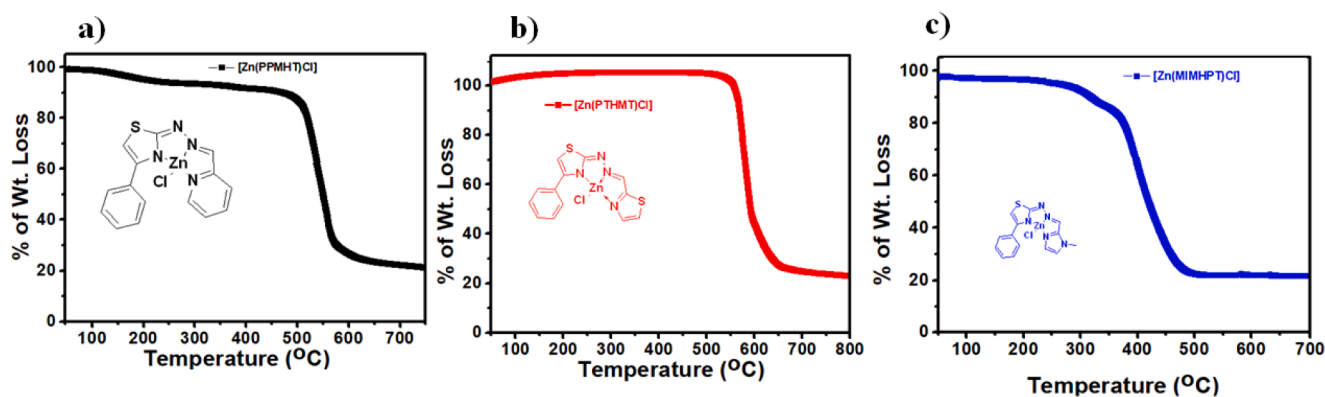


Fig. 1. Thermograms of a) [Zn(PPMHT)Cl], b) [Zn(PTMHT)Cl] and c) [Zn(MIMHPT)Cl] complexes.

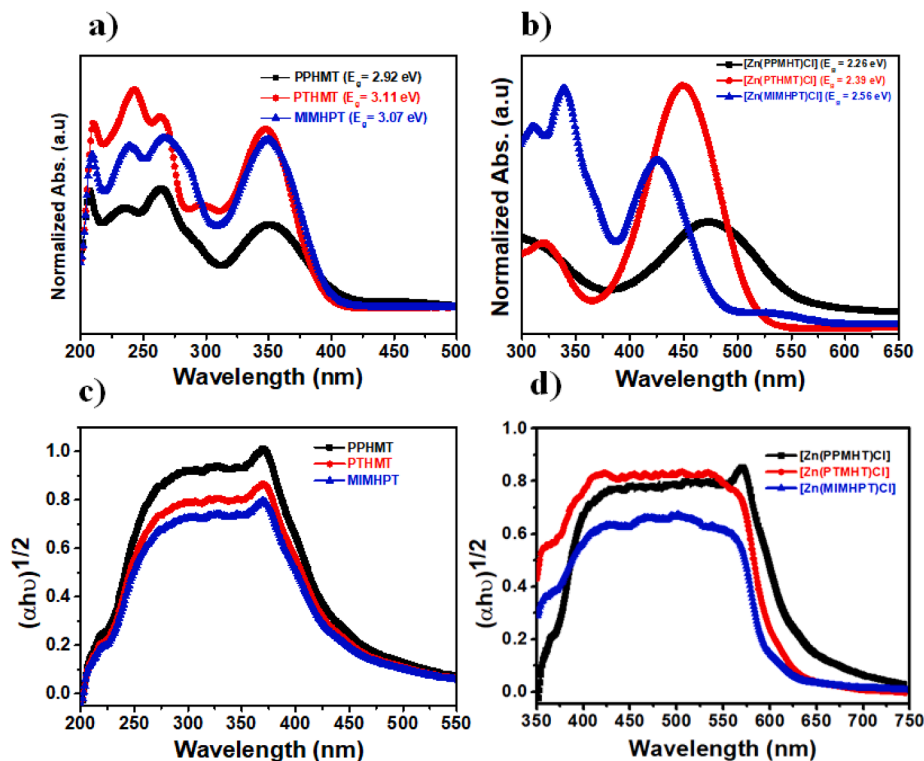


Fig. 2. a) and b) UV-visible spectra of ligands PPMHT, PTMHT and MIMHPT and [Zn(PPMHT)Cl], [Zn(PTMHT)Cl] and [Zn(MIMHPT)Cl] complexes in solution phase; c) and d) UV-vis DRS spectra of ligands and Zn (II) complexes.

Table 2
Optical properties and HOMO-LUMO energies of ligands and Zn (II) complexes (Experimental and calculated).

Ligand/complex	λ_{\max} (nm)	Calcd. λ_{\max} (nm)	λ_{onset} (nm) Solution/solid	HOMO-LUMO gap (eV)		TD-DFT
				Experimental		
				Solution phase	Solid state	
PPMHT	264, 348	304, 410	416/500	2.98	2.48	3.28
PTMHT	266, 352	313, 422	398/473	3.11	2.62	3.37
MIMHPT	268, 356	289, 369	403/449	3.07	2.76	3.68
[Zn(PPMHT)Cl]	322, 476	348, 485	578/574	2.14	2.16	2.79
[Zn(PTMHT)Cl]	328, 452	339, 471	512/508	2.42	2.44	2.80
[Zn(MIMHPT)Cl]	338, 426	316, 436	476/469	2.61	2.64	3.08

To get better understanding in the observed absorption energies, DFT and TD-DFT calculations were carried out by using Gaussian 16 software [29]. The method DFT/B3LYP/6-31G (d, p) is used for the optimization of simple syn and anti-isomers of PPMHT, PTMHT, and MIMHPT ligands, this method is previously applied to analogous heterocyclic ligands [28]. Due to presence of double bond between N and C, each ligand exists in two isomeric forms (syn and anti). Syn and anti-isomers also exists in other configurations due to the N-C single bond rotation. The relative energies of isomers/ configurations of ligands are shown in Table S1 (SI). In all the ligands, the syn isomer is more stable than the anti-isomer due to the formation hydrogen bond. The existing calculated technique effectively repeats experimentally noticed development of the intramolecular H-bond between N1 of the imidazole/thiazole/pyridine ring and the proton present on the hydrazone group CH=N-NH- [28]. This result can be described by the existence of the stabilizing effect in the syn-isomeric form because of the intramolecular H-bond formation [30]. Further, to estimate the geometry of Zn (II) complexes we have applied, B3LYP method with 6-31G (d, p) basis set on ligand part and LANL2DZ basis set on Zn. The optimized Zn (II) complexes are shown in Table S2.

The estimation of absorption spectra and transition energies was supported out within the time dependent density functional theory (TD-DFT) technique, using the B3LYP functional. The calculated absorption spectra of simple ligands exhibit a shoulder band in between 250 and 300 nm and another band at 325–380 nm. Theoretically obtained absorption transitions (λ), oscillator strengths (f) and major MO contributions of the ligands are given in Table S3 (SI). The absorption peak in the range 250–300 nm is because of the π - π^* transition of phenyl and

imidazole/thiazole/ pyridine rings [30]. The azomethine group of ligands exhibited λ_{\max} in between 325 and 380 nm agrees to the π - π^* transition of the azomethine moiety [30] with an influence of the intraligand π - π^* transitions. The wavelengths initiating from π - π^* transitions of phenyl and imidazole/thiazole/pyridine rings, as well as azomethine group, are in well matched with experimental values (Table 2). E_{gap} values of the ligands obtained from λ_{\max} by the TD-DFT technique are also in agreement with the values estimated through UV-Vis spectroscopy (Table 2).

Graphical presentations of the theoretical HOMO, LUMO and HOMO-LUMO transitions for ligands and Zn (II) complexes are shown in Fig. 3. The HOMOs of PPMHT, PTMHT and MIMHPT ligands are delocalized mostly at the imine group, pyridine/thiazole/imidazole and phenyl rings, however the LUMOs are delocalized on the pyridine/thiazole/imidazole ring, the azomethine group and the core thiazole ring. Dynamically the most favorable π - π^* absorptions (400–525 nm) occur from HOMO \rightarrow LUMO transitions (Table S3, SI). Meanwhile the intraligand (π - π^*), ligand to metal charge transfer (LMCT), or spin-allowed transitions may originate due to enlargement of d-d bands [31–34].

In general, catalytic activity of a material depends on the surface area, higher surface area catalyst performs higher catalytic activity. Therefore, the surface area of the ligands and complexes were estimated through BET surface analyzer, plots were shown in Fig. S16 and presented in Table 3. Surface area of the Zn (II) complexes are very high as compared with its respective ligand, which gave a valuable evidence that the Zn (II) complexes are highly active materials for catalytic applications [13].

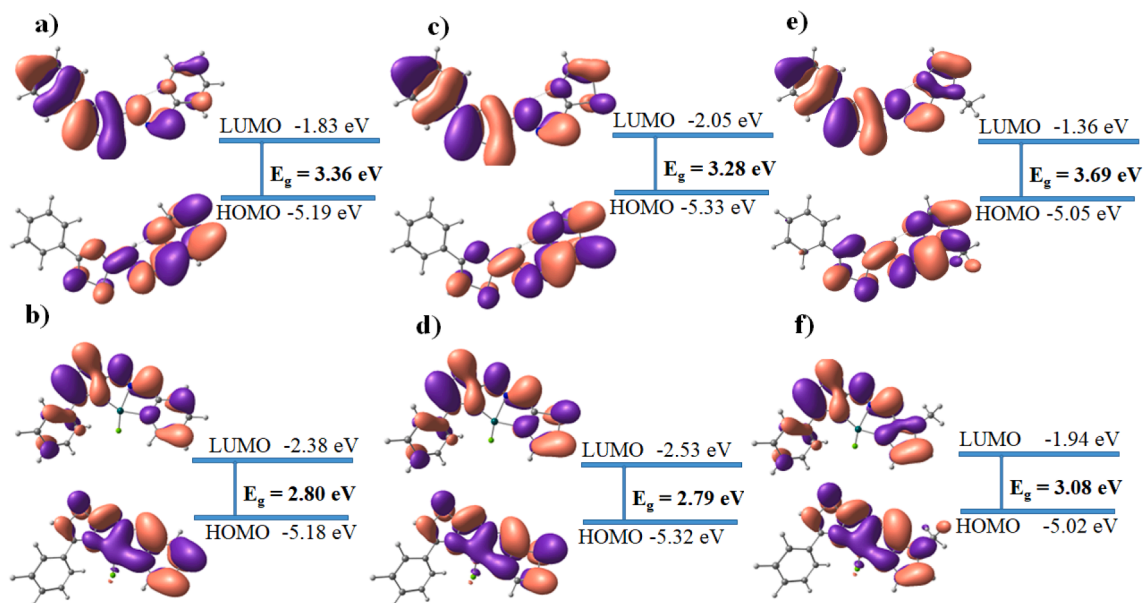


Fig. 3. Graphical presentation of theoretically obtained HOMO, LUMO and bandgap energy of ligands and Zn (II) complexes in DMF solvent.

Table 3
Surface area of ligands and Zn(II)-complexes.

Compound	Surface area (m ² /g)
PPMHT	13.314
PTMHT	21.282
MIMHPT	14.642
[Zn(PPMHT)Cl]	98.577
[Zn(PTMHT)Cl]	58.356
[Zn(MIMHPT)Cl]	44.291

The structural morphology of ligands and Zn (II) complexes were estimated through FESEM analysis. Metaphors of ligands and Zn (II) complexes completely altered as compared to each other. The shape of the particles of ligands such as PPMHT, PTMHT and MIMHPT were nanoflakes and nanoplates. In the case of Zn(II) complexes morphologies of each complex such as [Zn(PPMHT)Cl], [Zn(PTMHT)Cl] and [Zn(MIMHPT)Cl] are nanosticks, and nanoribbons [22] respectively is shown in Fig. 4.

Estimation of photoluminescence (PL) spectra of the Zn (II) complexes were carried out to know the rate of recombination of electron-hole (e⁻-h⁺) pair or charge separation of e⁻-h⁺. Intensity of the emission spectra of a complex is higher indicate fast rate of recombination of e⁻-h⁺ and vice-versa [35]. PL spectra of complexes were also confirmed in the solid state and the materials were excited at 410 nm, 405 nm and 395 for [Zn(PPMHT)Cl], [Zn(PTMHT)Cl] and [Zn(MIMHPT)Cl] complexes respectively, through slit width of 2 nm. In the present case, [Zn(PPMHT)Cl] showed lower emission intensity as compared to other two [Zn(PTMHT)Cl] and [Zn(MIMHPT)Cl] complexes. The quantum efficiency of [Zn(PPMHT)Cl], [Zn(PTMHT)Cl] and [Zn(MIMHPT)Cl] are 0.06, 0.18 and 0.34% respectively. Which indicate that [Zn(PPMHT)Cl] complex is more efficient for the separation of e⁻-h⁺ and low rate of recombination of e⁻-h⁺ pair (shown in Fig. S17).

3.1. Voltammetric and spectroelectrochemical studies

To know the oxidation potentials and overlapping of orbitals, all the ligands and its metal complexes were voltammetrically investigated in CH₃CN/C₂H₄Cl₂ (1:1 ratio, 0.05 molL⁻¹) using tetrabutylammonium hexafluorophosphate (NBu₄PF₆) as a supportive electrolyte. In the accessible potential range (-2.0 V to +2.0 V), the ligands exhibited primarily one oxidation and reduction peaks with well-known method (Fig. S18a – S18f). The reduction potential for each ligand molecule is placed in a 1-e⁻ wave around -1.0 V. This is related with the ligands, which upon complexation with a Zn²⁺ ions, the reduction potential is moved towards more negative side, which is corresponding to [Zn(PPMHT)Cl], [Zn(PTMHT)Cl] and [Zn(MIMHPT)Cl] and are given in Table 4.

The insitu spectro-electrochemistry of [Zn(PPMHT)Cl] was achieved in solution to estimate the spectral variations in its reduced state and compared with initial state (neutral). This is a significant method for identifying in further aspects of the electrochemical methods [28,36]. The complex [Zn(PPMHT)Cl] shows two electron changeable reduction waves at -1.04 V and -1.68 V. It is examined its spectral variations for first reduction state.

The insitu electronic spectra of [Zn(PPMHT)Cl] complex was established for first reduction potential at -1.04 V with regular interval of time. Remarkably, the observation of the absorption exhibited a very

Table 4
Voltammetric characteristics of the complexes.

Compound	E _{red} (I) (V)	E _{red} (II) (V)
PPMHT	-1.1036	-
PTMHT	-1.1321	-
MIMHPT	-0.9431	-
[Zn(PPMHT)Cl]	-1.1442	-1.7308
[Zn(PTMHT)Cl]	-1.2004	-1.5921
[Zn(MIMHPT)Cl]	-1.0888	-1.4549

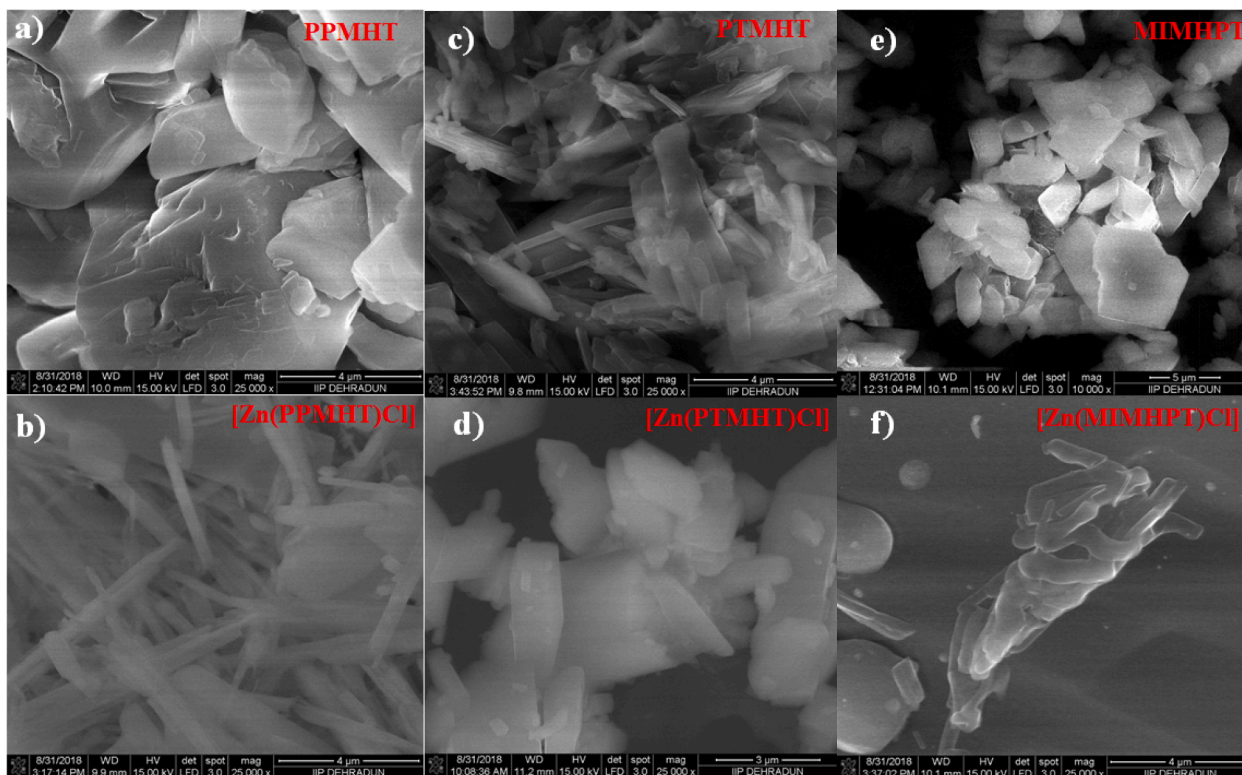


Fig. 4. Metaphors of both the ligands and Zn (II) complexes.

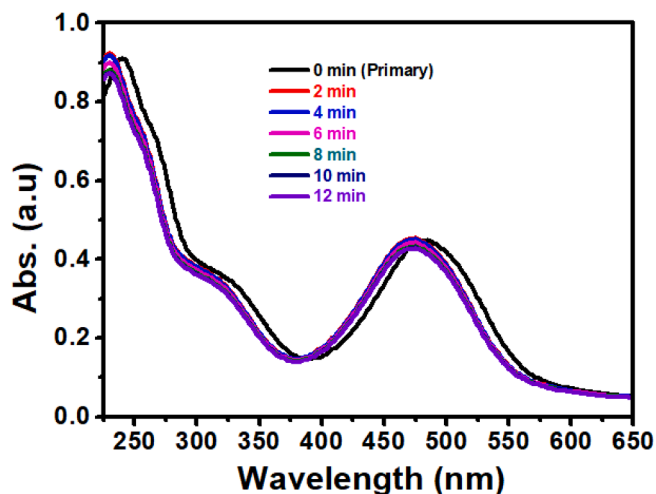


Fig. 5. Time determined electronic spectral variations of $[Zn(PPMHT)Cl]$ in deoxygenated $CH_3CN/C_2H_4Cl_2$ with 0.1 M NBu_4PF_6 initial and later applying the first reduction potential -1.05 V.

slow and slight change of the electronic transitions after the primary reduction (shown in Fig. 5). As revealed in Fig. 5, the foremost band cresting primarily at 483 nm is disturbed upon the primary electrocyclic (cathodic) reaction (first reduction i.e., -1.04 V). In fact, the observed band showed an hypsochromic shift, when compared with its non-reduced state (neutral state). The second intense band at 240 nm inclines to move towards lower wavelength region and slightly decreased its absorbance, which indicate that the foremost band at 483 nm of the initial $[Zn(PPMHT)Cl]$ complex was assigned to the ligand to metal charge transfer transition (LMCT). The two reduction peaks generate the Zn (II) and then Zn (I) from the primary Zn (II) ion so it makes the LMCT transition more tough. It clarifies that this foremost band was noticed at a higher wavelength related with that of the primary complex [28]. The opto-electrochemical tests reveal that the cathodic reactions resemble to

two sequential lone-electron reduction of the fundamental Zn (II) complex.

3.2. Photocatalysis

After confirmation of 1:1 ratio of Zn ions and ligands, the complexes are directly used as photocatalysts for photo-fragmentation of methyl orange (MO) and methyl violet (MV) dyes and photooxidation of methyl arenes and under visible light irradiation conditions.

3.3. Photo-fragmentation of organic dye pollutants (ODPs)

In general, most of the investigations ODPs are based on photo-degradation or photomineralization process in the presence of metal complexes, metal-organic frameworks, metal oxides (binary and ternary systems) under visible light irradiation conditions [23,37,38]. Some of the research studies showed that fragmentation of ODPs under visible light as source for photocatalysis process and these fragments also stable byproducts and source for new kind of pollutants [39]. In this work, focused on a new technique such as mild photo-catalysis in the presence of new Zn (II) complexes for conversion of ODPs into stable fragments of simple molecules with biodegradable nature. The biodegradable small molecules are identified through NMR and mass spectral studies. For optimization of method, both the anionic and cationic dyes (MO and MV) were selected and the outcomes were presented with the mean data with standard deviations as shown in Fig. S19.

The photo-catalytic activity of reported complexes is examined by the photo-fragmentation of MO and MV under the visible light irradiation. The sequential difference in MO and MV concentration with irradiation time in absence and presence of metal complexes is shown in Fig. 6. It is observed that MO and MV undergoes photo-fragmentation to the amount of 1% in the non-existence of the photocatalyst which may be because of photolysis. Nevertheless, in the occurrence of photocatalyst, the percentage of photo-fragmentation of MO (MV) dye is 89%, 80%, and 73% (99%, 61% and 31%) for $[Zn(PPMHT)Cl]$, $[Zn(PTMHT)Cl]$ and $[Zn(MIMHPT)Cl]$ respectively, with continuous irradiation of

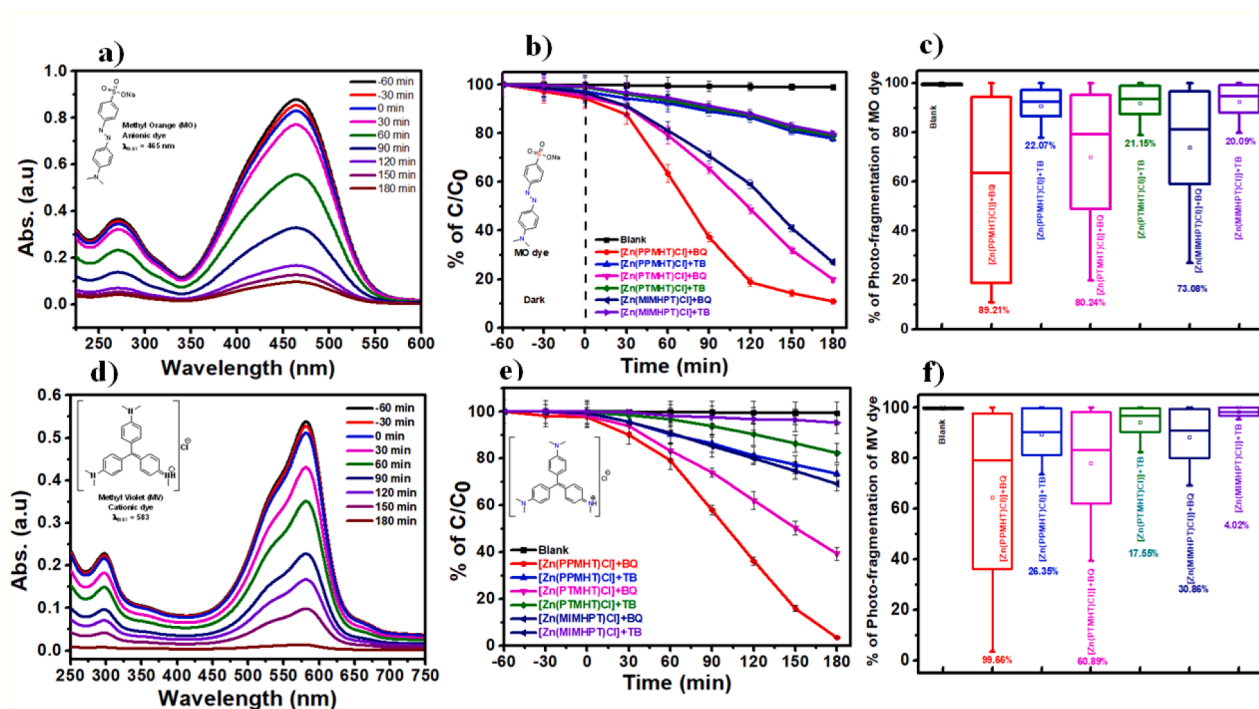


Fig. 6. a), d) successive absorbance spectral pattern for $[Zn(PPMHT)Cl]$, b), e) Photo-fragmentation of MO and MV and c), f) box chart plot for % of dye Photo-fragmentation in the presence of $[Zn(PPMHT)Cl]$, $[Zn(PTMHT)Cl]$ and $[Zn(MIMHPT)Cl]$ under visible light irradiation.

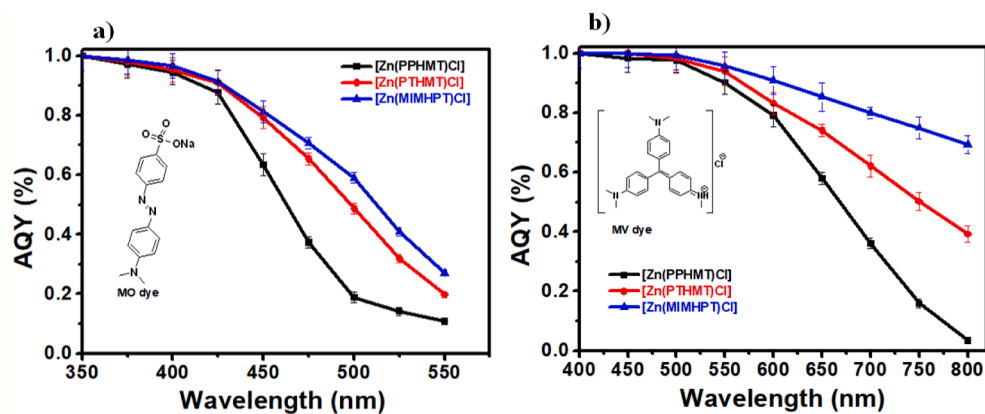


Fig. 7. Action spectra for a) Zn(II) complex photo-fragmentation of MO dye b) Zn(II) complex photo-fragmentation of MV dye under visible light irradiation.

visible light for 180 min and shown in action spectra Fig. 7. Therefore, these results indicate that photocatalytic performance of [Zn(PPMHT)Cl] is higher as compared with other two complexes such as [Zn(PTMHT)Cl], and [Zn(MIMHPT)Cl] due to high surface area and low bandgap energy. Hence, in the current study, [Zn(PPMHT)Cl] complex reveals better photocatalytic performance against MO and MV photo-fragmentation related to other two [Zn(PTMHT)Cl] and [Zn(MIMHPT)Cl] complexes. Some of the important fragments were identified through MS technique and presented in Table S4 and mass spectra shown in S20–S26. Examined some other parameters such as pH and strength of ions for a polluted dye water before and after exposure to visible light irradiation and shown in Table S5.

3.4. Photo decomposition of FIWW

The samples collected from various FIWW are verified with LC-MS method and information showed a wide-range of various m/z values as revealed in Fig. S27. From this data, several significant m/z values are recognized and coincide with the molecular weight of antioxidant compounds from oil mill wastewater (Fig. S27 and tentative structures as shown Fig. 8) and the remaining m/z values are unknown compounds

that were obtained by the food processing procedures. After primary study, the FIWW samples are subjected to visible light treatment in the existence of [Zn(PPMHT)Cl] catalyst. At that point, the samples are collected in a regular point of time for estimation of the amount of sample decomposed through UV-vis spectra. The information exhibited that the concentration of oil-based polyphenols was progressively reduced as shown in Fig. 9 and action spectra Fig. 10. Subsequently 180 min entirely mineralized the polyphenols and unknown compounds existing in the FIWW samples as revealed in Fig. 8. The final sample, oil-based solution was again estimated with LC-MS intense peaks are vanished as correlated with original data (Figs. S28 and S29). Therefore, [Zn(PPMHT)Cl] complex efficiency in the direction of the photodegradation of FIWW is greater than other two [Zn(PTMHT)Cl] and [Zn(MIMHPT)Cl] complexes. Finally, the photo decomposed FIWW achieved was studied for chemical oxygen demand (COD) test with $\text{Na}_2\text{Cr}_2\text{O}_7$ as the oxidizing agent and COD concentration ranged from 1200 to 10,000 mg/L. Fig. S30 displays the plot between COD and photo decomposition time. The COD of the FIWW reduced with increased time intervals. After 180 min of the action of visible light irradiation, the COD value exhibit a minimum COD value reduced by 92% [13]. Walkley and Black's technique [40] has been used as standard technique for estimating organic

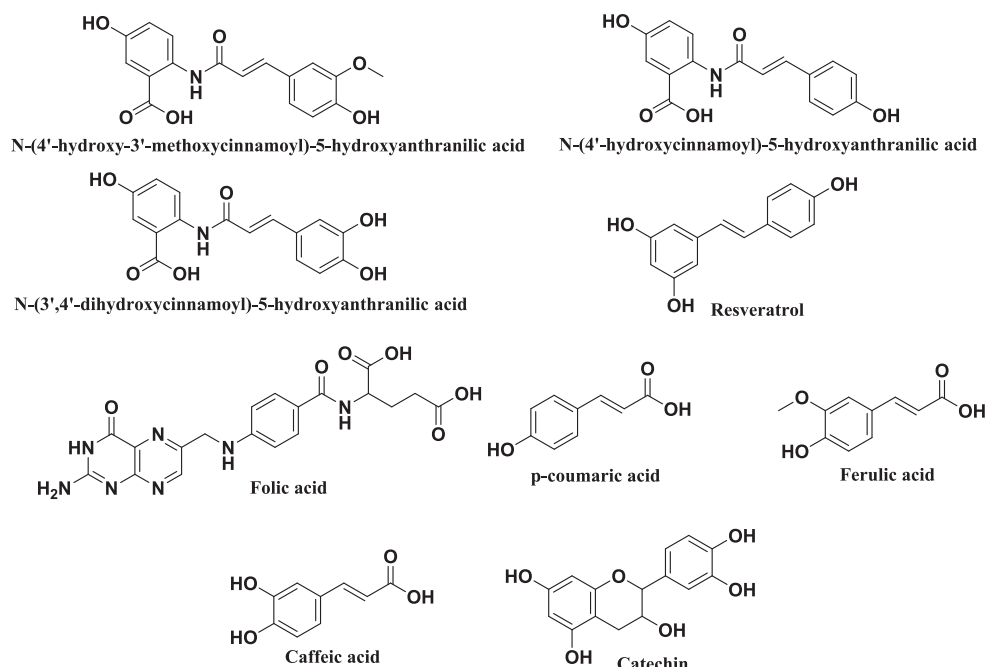


Fig. 8. Tentative chemical structures identified in FIWW sample through LC-MS data.

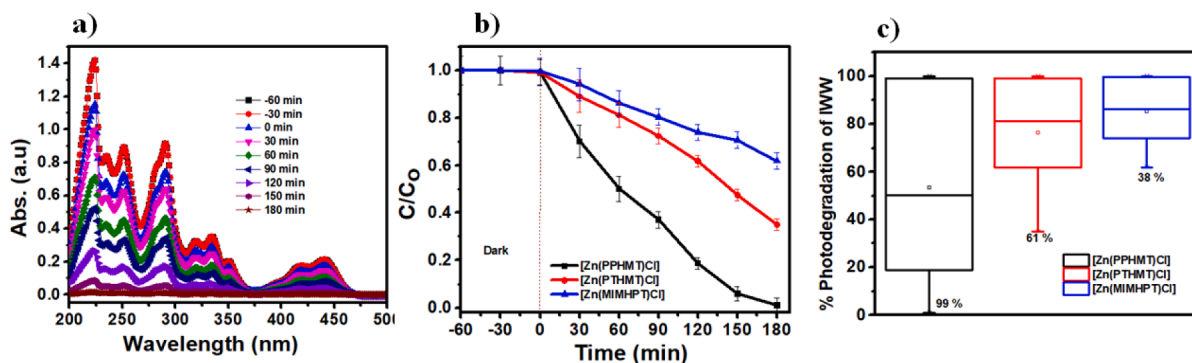


Fig. 9. a) successive absorbance spectral pattern for [Zn(PPMHT)Cl]; b) Photo decomposition of FIWW and c) box chart plot for % of Photo decomposition of FIWW in the presence of [Zn(PPMHT)Cl], [Zn(PTMHT)Cl] and [Zn(MIMHPT)Cl] under visible light irradiation.

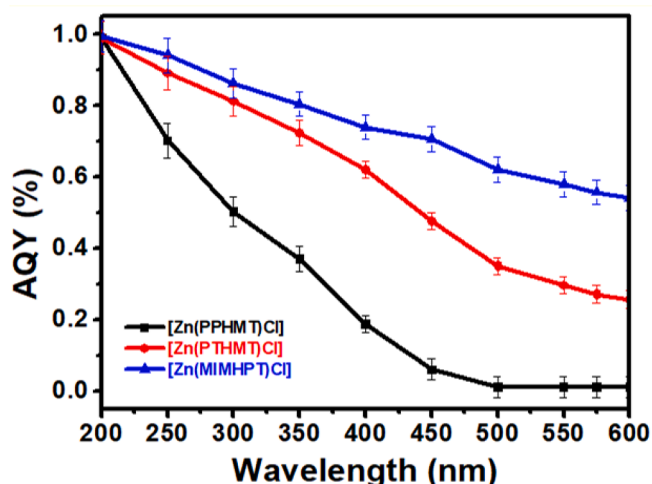


Fig. 10. Action spectra for a) Zn(II) complex photo-decomposition of FIWW under visible light irradiation.

carbon is changed to carbon dioxide (CO₂) in FIWW samples with various intervals of time were shown in Fig. S30. Estimating organic carbon is changed to carbon dioxide (CO₂), TOC can be obtained through COD (COD = 7.25 + 2.99*TOC) for every photodegraded sample with different time intervals [41].

3.5. Kinetics of Photo-fragmentation process

The kinetics of the photo-fragmentation process of dyes MO and MV in the presence of [Zn(PPMHT)Cl], [Zn(PTMHT)Cl] and [Zn(MIMHPT)Cl] complexes using logarithmic concentration with time given rate constant values are shown in Fig. S31. The order of rate constant of metal complexes are; [Zn(PPMHT)Cl] > [Zn(PTMHT)Cl] > [Zn(MIMHPT)Cl], which indicate that [Zn(PPMHT)Cl] complex exhibited higher photocatalytic performance than [Zn(PTMHT)Cl] and [Zn(MIMHPT)Cl]. Therefore, the decrease in absorbance intensity of the bands was observed throughout visible light irradiation in the existence of all the complexes. The kinetic outcomes stated in Fig. S31 reveal that the maximum performance photocatalyst is [Zn(PPMHT)Cl₂] and consist pyridine ligand has strong coordination with Zn(II) ions, which is one of the advantageous to increase the photocatalytic performance. Furthermore, ligand framework is highly favorable for binding with Zn(II) ions, enhances the kinetics of photo-fragmentation of dyes. It can be seen observation that the presence of pyridine ring with donor atoms have strong complexation ability with Zn(II) ions, which in turn increases the rate of photoreaction compared to other two complexes based on thiazole and imidazole rings. Though, alternative proposal is

the high performance of [Zn(PPMHT)Cl] is due to low rate of recombination charge and increasing the separating of (h⁺/e⁻) pairs accessible for photo-fragmentation of dyes.

3.6. Photooxidation of methyl arenes

Oxidation of alkyl arenes are the major challenging task in the heterogeneous catalysis (Scheme 2). In general, oxidation of primary alcohols is very easy in the presence of simple oxidation reagents such as MnO₂, PCC, PDC and Swern oxidation, Corey-Kim oxidation, Dess-Martin oxidation, CrO₃ and peroxides are used [42,43]. In all these processes, purification of products is very lengthy techniques due to the formation of number of byproducts. Therefore, a new photocatalyst is designing new Schiff's base Zn (II) complexes. Our previous work focused on C—H bond activation for synthesis of fused heterocyclic compounds and allylic oxidation in presence of Schiff's base complexes [44,45]. Present work mainly focused on oxidation of substituted alkyl arenes in the presence of new Zn-complexes. Optimization of new photocatalysts with commercially available complexes used for oxidation process and given in Table 5 and shown in Fig. S32.

After the optimization of reaction conditions various substituted methyl arenes and dimethyl arenes converted into respective aldehyde. All the xylenes under photooxidation process converted into dial whereas o-xylenes are converted to phthalaldehyde as major product and o-methyl benzaldehyde as very minor product. In the case of m-xylene and p-xylene no minor product was observed such as m-methyl benzaldehyde / p-methyl benzaldehyde only dial is exclusively formed in the presence of new Zn-complex system and inserted into Table 6.

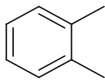
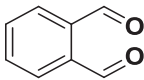
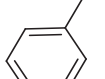
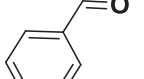
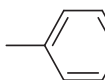
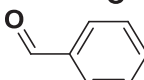
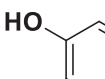
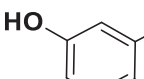
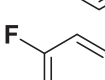
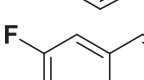
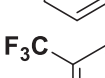
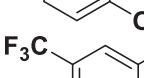
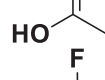
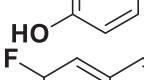
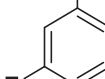
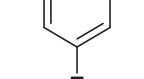
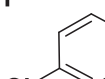
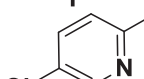
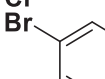
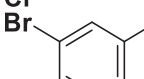
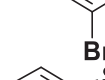
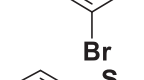
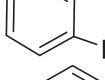
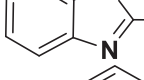
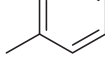
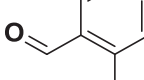
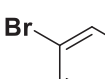
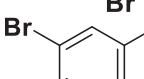
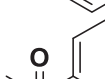
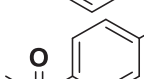
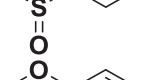
Table 5

Optimization of photocatalyst (PC) for conversion of p-xylene into terephthalaldehyde with various commercially available and new Zn(II) complexes.

S. No.	Photocatalyst	Time (h)	Yield (%) ^a
PC-1	Dichloro(N,N,N',N'-tetramethylethylenediamine) zinc (28308-00-1)	8/24	-/19
PC-2	Zinc bis[bis(trimethylsilyl)amide] (14760-26-0)	8/24	-/5
PC-3	Zinc di[bis(trifluoromethylsulfonyl)imide] (168106-25-0)	8/24	-/8
PC-4	Ziram (CAS No. 137-30-4)	8/24	12/28
PC-5	Zinc phthalocyanine (14320-04-8)	8/24	15/42
PC-6	[Zn(PPMHT)Cl]	8/24	85/92
PC-7	[Zn(PTMHT)Cl]	8/24	56/71
PC-8	[Zn(MIMHPT)Cl]	8/24	52/68

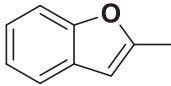
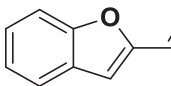
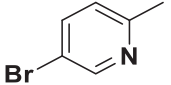
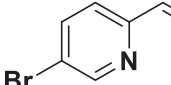
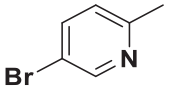
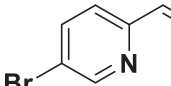
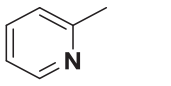
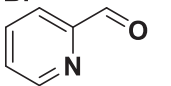
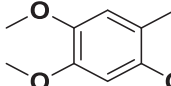
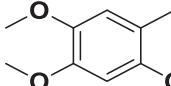
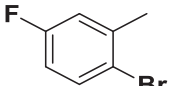
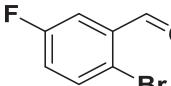
^a LC-MS analysis

Table 6
Photooxidation of various methyl arenes in the presence of Zn (II) complexes.

Entry	Starting Material	Product	Catalyst	Time (hours)	Yield (%)
1			[Zn(PPMHT)Cl]	8	66
			[Zn(PTMHT)Cl]		44
			[Zn(MIMHPT)Cl]		36
2			[Zn(PPMHT)Cl]	8	72
			[Zn(PTMHT)Cl]		48
			[Zn(MIMHPT)Cl]		42
3			[Zn(PPMHT)Cl]	8	85
			[Zn(PTMHT)Cl]		56
			[Zn(MIMHPT)Cl]		52
4			[Zn(PPMHT)Cl]	8	73
			[Zn(PTMHT)Cl]		49
			[Zn(MIMHPT)Cl]		44
5			[Zn(PPMHT)Cl]	8	75
			[Zn(PTMHT)Cl]		56
			[Zn(MIMHPT)Cl]		49
6			[Zn(PPMHT)Cl]	8	79
			[Zn(PTMHT)Cl]		56
			[Zn(MIMHPT)Cl]		51
7			[Zn(PPMHT)Cl]	8	76
			[Zn(PTMHT)Cl]		52
			[Zn(MIMHPT)Cl]		46
8			[Zn(PPMHT)Cl]	8	77
			[Zn(PTMHT)Cl]		58
			[Zn(MIMHPT)Cl]		51
9			[Zn(PPMHT)Cl]	8	83
			[Zn(PTMHT)Cl]		56
			[Zn(MIMHPT)Cl]		49
10			[Zn(PPMHT)Cl]	8	71
			[Zn(PTMHT)Cl]		53
			[Zn(MIMHPT)Cl]		46
11			[Zn(PPMHT)Cl]	8	82
			[Zn(PTMHT)Cl]		55
			[Zn(MIMHPT)Cl]		48
12			[Zn(PPMHT)Cl]	8	79
			[Zn(PTMHT)Cl]		51
			[Zn(MIMHPT)Cl]		45
13			[Zn(PPMHT)Cl]	8	68
			[Zn(PTMHT)Cl]		47
			[Zn(MIMHPT)Cl]		41
14			[Zn(PPMHT)Cl]	8	88
			[Zn(PTMHT)Cl]		62
			[Zn(MIMHPT)Cl]		53
15			[Zn(PPMHT)Cl]	8	72
			[Zn(PTMHT)Cl]		51
			[Zn(MIMHPT)Cl]		39
16			[Zn(PPMHT)Cl]	8	81
			[Zn(PTMHT)Cl]		54
			[Zn(MIMHPT)Cl]		43

(continued on next page)

Table 6 (continued)

Entry	Starting Material	Product	Catalyst	Time (hours)	Yield (%)
17			[Zn(PPMHT)Cl]	8	79
			[Zn(PTMHT)Cl]		53
			[Zn(MIMHPT)Cl]		47
18			[Zn(PPMHT)Cl]	8	67
			[Zn(PTMHT)Cl]		45
			[Zn(MIMHPT)Cl]		34
19			[Zn(PPMHT)Cl]	8	71
			[Zn(PTMHT)Cl]		52
			[Zn(MIMHPT)Cl]		40
20			[Zn(PPMHT)Cl]	8	82
			[Zn(PTMHT)Cl]		59
			[Zn(MIMHPT)Cl]		48
21			[Zn(PPMHT)Cl]	8	79
			[Zn(PTMHT)Cl]		47
			[Zn(MIMHPT)Cl]		39
22			[Zn(PPMHT)Cl]	8	73
			[Zn(PTMHT)Cl]		54
			[Zn(MIMHPT)Cl]		41

C—H bond activation of a variety of methylarenes was examined using 1.00 mol% of Zn(II) complexes 0.6 equiv. of $K_2S_2O_8$ (KSO) in CH_3CN/H_2O (1:1) under visible light treatment (Table 6). All the substrates were converted into the corresponding aldehydes with outstanding yields with a typical reaction time in the existence of [Zn(PPMHT)Cl] when related with the other two [Zn(PTMHT)Cl] and [Zn(MIMHPT)Cl] complexes as shown in Fig. S33.

3.7. Photostability and reusability studies

The photostability and photo-reusability of catalyst [Zn(PPMHT)Cl] was studied by collecting it from photoreaction mixture... It was noted that the [Zn(PPMHT)Cl] catalyst continued as same dark orange solid, suggesting that dye pollutants were not adsorbed on the top of the [Zn(PPMHT)Cl] catalyst and the total dyes are photo-fragmentated, which is established from 1H NMR of the complex, as matched with pure complex data (Fig. S34). Continuous reuse of [Zn(PPMHT)Cl] catalyst after three runs of photodegradation of MO and MV dyes, the [Zn(PPMHT)Cl] complex was centrifuged from photoreaction mixture and recorded 1H NMR spectra. From the spectral data it is established that the [Zn(PPMHT)Cl] complex is high photostable up to three cycles (shown Fig. S35).

3.8. Identification of active species for photo-fragmentation and photooxidation processes

In any photocatalytic process, active species are hydroxyl radical ($\cdot OH$), superoxide radical ($O_2\cdot^-$), hole (h^+) and electron (e^-) [22,46,47]. In order to interpret the possible mechanism for the photo-fragmentation of MO and MV dyes by using various scavengers (equimolar quantity with respect to catalyst) were assorted in the photoreaction. The effect of some scavengers on the photo-fragmentation of MO/MV is shown in Fig. 11a. The existence of electron ($Na_2S_2O_8$), superoxide (benzoquinone (BQ)), hole (ammonium oxalate) scavengers does not disturb the rate of photo-fragmentation of MO/MV noticeably, which gives a valuable information on photocatalytic process, and is not depends on electron, hole and superoxide radical ion. Whereas, when t-butyl alcohol used as a scavenger for hydroxyl radical, then considerable drop in the reaction rate is observed. Which indicate that $\cdot OH$ radicals are active species for photo-fragmentation process. Similarly, the mechanism for photooxidation of methyl arenes has been proposed through hydroxyl radicals in the presence of Zn-complexes, shown in Fig. 11a.

Further evidence for the $\cdot OH$ radicals as active species for the both photo-fragmentation and photooxidation were examined through the photocatalytic hydroxylation of terephthalic acid (TA) [23]. It is familiar that the $\cdot OH$ radicals react with TA and converts to 2-hydroxy

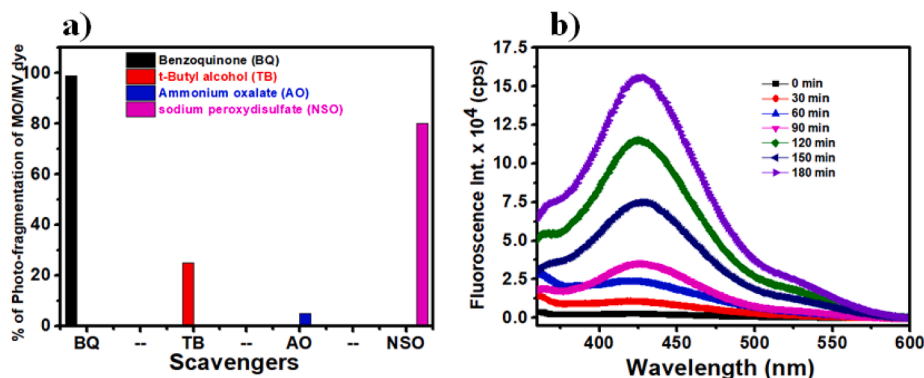


Fig. 11. a) Mechanistic Study for photo-fragmentation process for MO and MV dyes in the presence of various scavengers b) PL spectral enhances under visible light irradiation systematic time intervals on [Zn(PPMHT)Cl] complex in terephthalic acid.

terephthalic acid (TAOH), which emits a characteristic emission band at 440 nm. Photocatalytic study with TA was fixed out in the existence of Zn (II) complexes under visible light treatment (Fig. 11b). It is also noticed that with constant passage of visible light with regular time intervals, the intensity of emission band gradually increased [23]. Gradually, increase of emission band indicated that the amount of $\cdot\text{OH}$ radicals interacted with TA under visible light. This indicates, the $\cdot\text{OH}$ radicals are responsible for the photocatalytic performance of Zn (II) complexes.

4. Conclusions

New Zn-complexes such as [Zn(PPMHT)Cl], [Zn(PTMHT)Cl] and [Zn(MIMHPT)Cl] were synthesized from PPMHT, PTMHT and MIMHPT via complexation and characterized thoroughly by spectroscopic techniques. The photocatalytic fragmentation of the methyl orange and methyl violet dyes and photooxidation of methyl arenes with the prepared [Zn(PPMHT)Cl], [Zn(PTMHT)Cl] and [Zn(MIMHPT)Cl] photocatalysts were examined under visible light irradiation. The metal complex [Zn(PPMHT)Cl] giving the best photo-fragmentation and photooxidation performance, followed by [Zn(PTMHT)Cl] and then [Zn(MIMHPT)Cl]. The photocatalytic performance of the [Zn(PPMHT)Cl] complex towards photo-fragmentation of dyes established through Mass spectroscopy data. All the Zn (II) complexes acts as photocatalysts because of the excellent photostability. The hydroxyl radicals are showing the substantial influence on the photo-fragmentation of dyes and photooxidation of methyl arenes and which is established through scavenger and terephthalic acid probe methods. The improved photocatalytic performance of [Zn(PPMHT)Cl] was attributed to a smaller bandgap, high surface area and more charge separation of the holes and electrons.

Declaration of Competing Interest

The authors declare that they have no known competing financial interests or personal relationships that could have appeared to influence the work reported in this paper.

Acknowledgments

Authors would like to thank DST – FIST, schemes UGC (SAP) and SP for financial support under UGC-MRP 6417/16 (SERO/UGC), New Delhi. One of us JA thanks, UGC, New Delhi for the award of Junior Research Fellowship. PC thank to CSIR, New Delhi, India (02(0339)/18/EMR-II) for financial support.

Appendix A. Supplementary data

Supplementary data to this article can be found online at <https://doi.org/10.1016/j.jphotochem.2021.113455>.

References

- A.Z. El-Sonbati, W.H. Mahmoud, G.G. Mohamed, M.A. Diab, S.M. Morgan, S. Y. Abbas, Synthesis, characterization of Schiff base metal complexes and their biological investigation, *Appl. Organomet. Chem.* 33 (2019) 5048.
- Q. Wu, W.-L. Chen, D. Liu, C. Liang, Y.-G. Li, S.-W. Lin, E. Wang, New class of organic-inorganic hybrid aggregates based on polyoxometalates and Metal-Schiff-base, *Dalton Trans.* 40 (2011) 56–61.
- Y. Wu, J. He, S. Wang, L. Zou, X. Wu, Syntheses, crystal structure, and photocatalytic property of two new complexes of an unsymmetrical Schiff base ligand, *Inorg. Chim. Acta* 458 (2017) 218–223.
- M.S. More, P.G. Joshi, Y.K. Mishra, P.K. Khanna, Metal complexes driven from Schiff bases and semicarbazones for biomedical and allied applications: a review, *Mater. Today Chem.* 14 (2019), 100195.
- A. Wachi, Y. Kudo, A. Kanesaka, H. Nishikawa, T. Shiga, H. Oshio, M. Chikamatsu, R. Azumi, Organic field-effect transistor based on paramagnetic Cu(II) neutral complexes coordinated by Schiff base-type TTF ligands, *Polyhedron* 136 (2017) 70–73.
- C. Cheng, M. Brookhart, Iridium-catalyzed reduction of secondary amides to secondary amines and imines by diethylsilane, *J. Am. Chem. Soc.* 134 (2012) 11304–11307.
- M. Kaur, S. Kumar, S.A. Younis, M. Yusuf, J. Lee, S. Weon, K.-H. Kim, A.K. Malik, Post-synthesis modification of metal-organic frameworks using Schiff base complexes for various catalytic applications, *Chem. Eng. J.* 423 (2021) 130230, <https://doi.org/10.1016/j.cej.2021.130230>.
- Y. Ding, Y. Wu, T. Zhang, L. Tao, X. Liu, X. Liu, L. Hu, T. Hayat, A. Alsaedi, S. Dai, Colorful TiO_2 microspheres cooperating with titanium Schiff base complex for efficient visible light photocatalysts, *Catal. Today* 335 (2019) 550–556.
- J.F. Góngora-Gómez, P. Elizondo-Martínez, N. Pérez, M. Villanueva-Rodríguez, L. Hinojosa-Reyes, A. Hernández-Ramírez, Sensitization of TiO_2 with novel Cu(II) and Ni(II) polyaza complexes: evaluation of its photocatalytic activity, *Ceram. Inter.* 40 (2014) 14207–14214.
- V. Gugulothu, J. Ahemed, M. Subburu, B. Yadagiri, R. Mittal, C. Prabhakar, S. Pola, Evolution of physical and photocatalytic properties of new Zn(II) and Ru(II) complexes, *Polyhedron* 170 (2019) 412–423.
- G. R. Reddy, S. Balasubramanian, K. Chennakesavulu, Correction: Zeolite encapsulated Ni(ii) and Cu(ii) complexes with tetradentate N2O2 Schiff base ligand: catalytic activity towards oxidation of benzhydrol and degradation of rhodamine-B, *J. Mater. Chem. A*, 2 (2014) 19102–19102.
- J.L. Woodliffe, R.S. Ferrari, I. Ahmed, A. Laybourn, Evaluating the purification and activation of metal-organic frameworks from a technical and circular economy perspective, *Coord. Chem. Rev.* 428 (2021), 213578.
- M. Subburu, R. Gade, V. Guguloth, P. Chetti, K.R. Ravulapelly, S. Pola, Effective photodegradation of organic pollutants in the presence of mono and bi-metallic complexes under visible-light irradiation, *J. Photochem. Photobiol. A: Chem.* 406 (2021), 112996.
- S. Bibi, A. Ahmad, M.A.R. Anjum, A. Haleem, M. Siddiq, S.S. Shah, A. AlKahtani, Graphene Oxide (rGO) based Metal Oxides (rGO-Fe3O4/TiO2) Nanocomposite under UV-Visible Light Irradiation, *J. Environ. Chem. Eng.* (2021), 105580.
- P. Amornpitoksuk, S. Suwanboon, S. Kaowphong, C. Random, P. Graidist, Photocatalytic activity of $\text{K}_2\text{Ti}_6\text{O}_{13}/\text{TiO}_2$ nanocomposite prepared using water extract of wood ash from waste for degradation of dye pollutants, *J. Taiwan Inst. Chem. Eng.* 117 (2020) 242–251.
- E. Beyers, P. Cool, E.F. Vansant, Anatase formation during the synthesis of mesoporous titania and its photocatalytic effect, *J. Phys. Chem. B* 109 (20) (2005) 10081–10086.
- N.B.G. Reddy, P.M. Krishna, N. Kottam, Novel metal-organic photocatalysts: synthesis, characterization and decomposition of organic dyes, *Spectrochim. Acta A* 137 (2015) 371–377.
- D. Liao, C. Badour, B. Liao, Preparation of nanosized TiO_2/ZnO composite catalyst and its photocatalytic activity for degradation of methyl orange, *J. Photochem. Photobiol. A: Chem.* 194 (2008) 11–19.
- L. Lu, J. Wang, C. Shi, Y. Sun, W. Wu, Y. Pan, M. Muddassar, Four structural diversity MOF-photocatalysts readily prepared for the degradation of the methyl violet dye under UV-visible light, *New J. Chem.* 45 (2021) 551–560.
- S. Tripathi, S.N. Singha, L.D.S. Yadav, Visible light photocatalysis with CBr4: a highly selective aerobic photooxidation of methylarenes to aldehydes, *RSC Adv.* 6 (2016) 14547–14551.
- H. Elshafli, S. Bjelogrić, C.D. Muller, T.R. Todorović, M. Rodić, A. Marinković, N. R. Filipović, Co(III) complex with (E)-2-(2-(pyridin-2-ylmethylene)hydrazinyl)-4-(4-tolyl)-1,3-thiazole: structure and activity against 2-D and 3-D cancer cell models, *J. Coord. Chem.* 69 (2016) 3354–3366.
- V. Guguloth, J. Ahemed, M. Subburu, V.C. Guguloth, P. Chetti, S. Pola, A very fast photodegradation of dyes in the presence of new Schiff's base N_4 -macrocyclic Ag-doped Pd(II) complexes under visible-light irradiation, *J. Photochem. Photobiol. A: Chem.* 382 (2019), 111975.
- S. Pola, M. Subburu, R. Guja, V. Muga, Y.-T. Tao, New photocatalyst for allylic aliphatic C-H bond activation and degradation of organic pollutants: Schiff base Ti(IV) complexes, *RSC Adv.* 5 (2015) 58504–58513.
- Mohammad Azam, Zahid Hussain, Ismail Warad, Saud I. Al-Resayes, Mohd. Shahnawaz Khan, Mohammad Shakir, Agata Trzesowska-Kruszyska, Rafal Kruszynski, Novel Pd(II)-salen complexes showing high in vitro anti-proliferative effects against human hepatoma cancer by modulating specific regulatory genes, *Dalton Trans.* 41 (35) (2012) 10854, <https://doi.org/10.1039/c2dt31143g>.
- N. Rashidi, M.J.S. Fard, P. Hayati, J. Janczak, F. Yazdian, S. Rouhani, T.A. M. Msagati, Antibacterial and cytotoxicity assay of two new Zn(ii) complexes: synthesis, characterization, X-Ray structure, topology, Hirshfeld surface and thermal analysis, *J. Mol. Str.* 1231 (2021), 129947.
- K.A. Alim, V.A. Fonoberov, M. Shamsa, A.A. Balandin, Micro-Raman investigation of optical phonons in ZnO nanocrystals, *J. Appl. Phys.* 97 (2005), 124313.
- A.K. Mohamed, K.S. Islam, S.S. Hasan, M. Shakir, Metal ion directed synthesis of 14–16 membered tetraamine macrocyclic complexes, *Transit. Metal Chem.* 24 (1999) 198.
- N.R. Filipović, H. Elshafli, S. Grubišić, L.S. Jovanović, M. Rodić, I. Novaković, A. Malešević, I.S. Djordjević, H. Li, N. Šojić, A. Marinković, T.R. Todorović, Co(III) complexes of (1,3-selenazol-2-yl)hydrazones and their sulphur analogues, *Dalton Trans.* 46 (2017) 2910–2924.
- M.J. Frisch, G.W. Trucks, H.B. Schlegel, G.E. Scuseria, M.A. Robb, J.R. Cheeseman, G. Scalmani, V. Barone, B. Mennucci, G.A. Petersson, H. Nakatsuji, M. Caricato, X. Li, H.P. Hratchian, A.F. Izmaylov, J. Bloino, G. Zheng, J.L. Sonnenberg, M. Hada, M. Ehara, K. Toyota, R. Fukuda, J. Hasegawa, M. Ishida, T. Nakajima, Y. Honda, O. Kitao, H. Nakai, T. Vreven, J.A. Montgomery Jr., J.E. Peralta, F. Ogliaro, M. Bearpark, J.J. Heyd, E. Brothers, K.N. Kudin, V.N. Staroverov, R. Kobayashi, J.

- Normand, K. Raghavachari, A. Rendell, J.C. Burant, S.S. Iyengar, J. Tomasi, M. Cossi, N. Rega, J.M. Millam, M. Klene, J.E. Knox, J.B. Cross, V. Bakken, C. Adamo, J. Jaramillo, R. Gomperts, R.E. Stratmann, O. Yazyev, A.J. Austin, R. Cammi, C. Pomelli, J.W. Ochterski, R.L. Martin, K. Morokuma, V.G. Zakrzewski, G.A. Voth, P. Salvador, J.J. Dannenberg, S. Dapprich, A.D. Daniels, O. Farkas, J.B. Foresman, J.V. Ortiz, J. Cioslowski, D.J. Fox, Gaussian 09, Revision A.02, Gaussian, Inc., Wallingford CT, 2009.
- [30] E.B. Seena, M.R. Prathapachandra Kurup, Synthesis, spectral and structural studies of zinc (II) complexes of salicylaldehyde N (4)-phenylthiosemicarbazone, *Spectrochim. Acta Part A Mol. Biomol. Spectrosc.* 69 (3) (2008) 726–732.
- [31] Y.-W. Dong, R.-Q. Fan, P. Wang, L.-G. Wei, X.-M. Wang, S. Gao, H.-J. Zhang, Y.-L. Yang, Y.-L. Wang, Tunable luminescence and application in dye-sensitized solar cells of Zn(II)/Hg(II) complexes: methyl substitution-induced supramolecular structures based on (E)-N-(6-Methoxypyridin-2-ylmethylene)arylamine Derivatives, *Inorg. Chem.* 54 (2015) 7742–7752.
- [32] J. Gradinaru, A. Forni, V. Druta, F. Tessore, S. Zecchin, S. Quici, N. Garbalau, Structural, Spectral, Electric-Field-Induced Second Harmonic, and Theoretical Study of Ni(II), Cu(II), Zn(II), and VO(II) Complexes with [N₂O₂] Unsymmetrical Schiff Bases of S-Methylisothiosemicarbazide Derivatives, *Inorg. Chem.* 46 (2007) 884–895.
- [33] G. Consiglio, S. Failla, P. Finocchiaro, I. Pietro Oliveri, S.D. Bella, Aggregation properties of bis (salicylaldiminato) zinc (II) Schiff-base complexes and their Lewis acidic character, *Dal. Trans.* 41 (2012) 387–395.
- [34] I. Majumder, P. Chakraborty, S. Dasgupta, C. Massera, D. Escudero, D. Das, A Deep Insight into the Photoluminescence Properties of Schiff Base Cd (II) and Zn (II) Complexes, *Inorg. Chem.* 56 (2017) 12893–12901.
- [35] Dan Wang, Shu-Mu Li, Jian-Quan Zheng, Duan-Yang Kong, Xiang-Jun Zheng, De-Cai Fang, Lin-Pei Jin, Coordination-directed stacking and aggregation-induced emission enhancement of the Zn(II) Schiff Base Complex, *Inorg. Chem.* 56 (2) (2017) 984–990.
- [36] J. Losada, I. Del Peso, L. Beyer, Electrochemical and spectroelectrochemical properties of copper (II) Schiff-base complexes, *Inorg. Chim. Acta* 321 (2001) 107–115.
- [37] Sherif A. Younis, Eilhann E. Kwon, Muhammad Qasim, Ki-Hyun Kim, Taejin Kim, Deepak Kukkar, Xiaomin Dou, Imran Ali, Metal-organic framework as a photocatalyst: Progress in modulation strategies and environmental/energy applications, *Prog. Ener. & Comb. Sci.* 81 (2020) 100870, <https://doi.org/10.1016/j.pecs.2020.100870>.
- [38] J. Čirković, A. Radojković, D.L. Golić, N. Tasić, M. Čizmić, G. Branković, Z. Branković, Visible-light photocatalytic degradation of Mordant Blue 9 by single-phase BiFeO₃ nanoparticles, *J. Environ. Chem. Eng.* 9 (2021), 104587.
- [39] Sreed S. Kanakkillam, B. Krishnan, D.A. Avellaneda, S. Shaji, Surfactant free stable cobalt oxide nanocolloid in water by pulsed laser fragmentation and its thin films for visible light photocatalysis, *Coll. Surf. A: Physicochem. Eng. Aspects* 594 (2020) 124657, <https://doi.org/10.1016/j.colsurfa.2020.124657>.
- [40] M.D. Mingorance, E. Barahona, J. Fernández-Gálvez, Guidelines for improving organic carbon recovery by the wet oxidation method, *Chemosphere* 68 (3) (2007) 409–413.
- [41] D. Dubber, N.F. Gray, Replacement of chemical oxygen demand (COD) with total organic carbon (TOC) for monitoring wastewater treatment performance to minimize disposal of toxic analytical waste, *J. Environ. Sci. Health A Tox. Hazard. Subst. Environ. Eng.* 45 (2010) 1595–1600.
- [42] H.R. Mardani, H. Golchoubian, Selective and efficient C-H oxidation of alkanes with hydrogen peroxide catalyzed by a manganese (III) Schiff base complex, *J. Mol. Catal. A: Chem.* 259 (2006) 197–200.
- [43] W. Al Zoubi, Y.G. Ko, Organometallic complexes of Schiff bases: recent progress in oxidation catalysis, *J. Organometal. Chem.* 822 (2016) 173–188.
- [44] C.G. Newton, et al., Catalytic enantioselective transformations involving C-H bond cleavage by transition-metal complexes, *Chem. Rev.* 117 (2017) 8908–8976.
- [45] C. Feng, X. Yang, Z. Sun, J. Xue, Dual interfacial synergism in Au-Pd/ZnIn₂S₄ for promoting photocatalytic selective oxidation of aromatic alcohol, *Appl. Surf. Sci.* 501 (2020), 144018.
- [46] Penghui Shao, Jiayu Tian, Feng Yang, Xiaoguang Duan, Shanshan Gao, Wenxin Shi, Xubiao Luo, Fuyi Cui, Shenglian Luo, Shaobin Wang, Identification and regulation of active sites on nanodiamonds: establishing a highly efficient catalytic system for oxidation of organic contaminants, *Adv. Funct. Mater.* 28 (13) (2018) 1705295.
- [47] P. Shao, S. Yu, X. Duan, L. Yang, H. Shi, L. Ding, J. Tian, L. Yang, X. Luo, S. Wang, Potential difference driving electron transfer via defective carbon nanotubes toward selective oxidation of organic micropollutants, *Environ. Sci. Technol.* 54 (2020) 8464–8472.